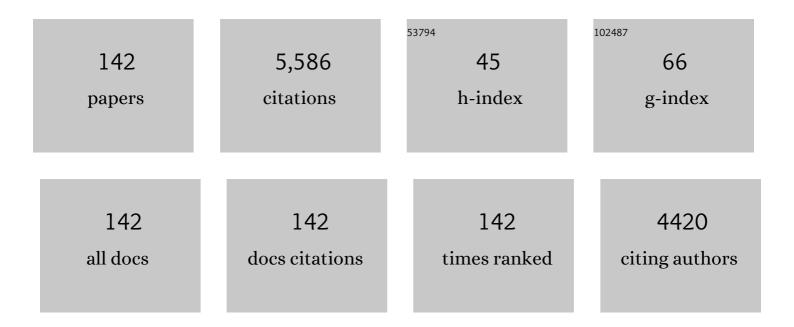
Chao Zhang

List of Publications by Year in descending order

Source: https://exaly.com/author-pdf/8304528/publications.pdf

Version: 2024-02-01



Снао 7намс

#	Article	IF	CITATIONS
1	Preparation of ZnO1-x by peroxide thermal decomposition and its room temperature gas sensing properties. Rare Metals, 2022, 41, 871-876.	7.1	19
2	Room temperature WO3-Bi2WO6 sensors based on hierarchical microflowers for ppb-level H2S detection. Chemical Engineering Journal, 2022, 430, 132813.	12.7	11
3	Role of ruthenium incorporation on room-temperature nonanal sensing properties of Ru-loaded urchin-like W18O49 hierarchical nanostructure. Sensors and Actuators B: Chemical, 2022, 353, 131096.	7.8	15
4	Low concentration isopropanol gas sensing properties of Ag nanoparticles decorated In2O3 hollow spheres. Journal of Advanced Ceramics, 2022, 11, 379-391.	17.4	56
5	Room-temperature gas sensors based on titanium dioxide quantum dots for highly sensitive and selective H2S detection. Applied Surface Science, 2022, 585, 152744.	6.1	20
6	Stability of Metal Oxide Semiconductor Gas Sensors: A Review. IEEE Sensors Journal, 2022, 22, 5470-5481.	4.7	56
7	Investigation on microstructure and nonanal sensing properties of hierarchical Sb2WO6 microspheres. Ceramics International, 2022, 48, 30249-30259.	4.8	12
8	Facile synthesis of bismuth ferrite nanoparticles for ppm-level isopropanol gas sensor. Journal of Materials Science: Materials in Electronics, 2022, 33, 18507-18521.	2.2	3
9	Volatile organic compounds gas sensor based on quartz crystal microbalance for fruit freshness detection: A review. Food Chemistry, 2021, 334, 127615.	8.2	71
10	A detailed analysis on the microstructure and compressive properties of selective laser melted Ti6Al4V lattice structures. Materials and Design, 2021, 198, 109292.	7.0	21
11	Synthesis and NH3/TMA sensing properties of CuFe2O4 hollow microspheres at low working temperature. Rare Metals, 2021, 40, 1768-1777.	7.1	33
12	A novel low-concentration isopropanol gas sensor based on Fe-doped ZnO nanoneedles and its gas sensing mechanism. Journal of Materials Science, 2021, 56, 3230-3245.	3.7	38
13	Microwave-assisted hydrothermal synthesis of copper oxide-based gas-sensitive nanostructures. Rare Metals, 2021, 40, 1477-1493.	7.1	48
14	Preparation and photocatalytic performance of TiO ₂ -RGO-CuO/Fe ₂ O ₃ ternary composite photocatalyst by solvothermal method. Materials Research Express, 2021, 8, 015025.	1.6	4
15	Electronic nose for volatile organic compounds analysis in rice aging. Trends in Food Science and Technology, 2021, 109, 83-93.	15.1	62
16	Cavitation Erosion Resistance of TiNi-Based Composite Coating Deposited by APS. Journal of Thermal Spray Technology, 2021, 30, 937-945.	3.1	1
17	Microstructure and Tribological Properties of Plasma-Sprayed CoCrFeNi-based High-Entropy Alloy Coatings Under Dry and Oil-Lubricated Sliding Conditions. Journal of Thermal Spray Technology, 2021, 30, 926-936.	3.1	29
18	Effects of Co addition on microstructure and cavitation erosion resistance of plasma sprayed TiNi based coating. Surface and Coatings Technology, 2021, 409, 126838.	4.8	4

#	Article	IF	CITATIONS
19	Structure and Photocatalytic Properties of In(OH) ₃ /InOOH Natural Heterojunction Nanocrystals Prepared by Hydrothermal Synthesis. Journal of Chemical Engineering of Japan, 2021, 54, 93-102.	0.6	0
20	Wear behaviors of 5Âwt % SiO2–Ni60 coatings deposited by atmospheric plasma spraying under dry and water-lubrication sliding conditions. Wear, 2021, 470-471, 203621.	3.1	11
21	Combining topography and peptide to inhibit algae attachment: Preparation of peptideâ€modified microstructured surfaces. Surface and Interface Analysis, 2021, 53, 973-981.	1.8	5
22	Effect of Pre-oxidation on High-Temperature Chlorine-induced Corrosion Properties of Air Plasma-Sprayed Ni-5%Al Coatings. Journal of Thermal Spray Technology, 2021, 30, 1927-1939.	3.1	8
23	Influence of water vapor on the chlorine-induced high-temperature corrosion behavior of nickel aluminide coatings. Corrosion Science, 2021, 190, 109689.	6.6	6
24	Oneâ€step synthesis of Cu/N coâ€doped TiO ₂ nanocomposites with enhanced photocatalytic activities under visibleâ€light irradiation. Micro and Nano Letters, 2021, 16, 573-581.	1.3	5
25	Room temperature NO2 sensing properties of ZnO1-α coating prepared by hydrogen reduction method. Ceramics International, 2021, 47, 29873-29880.	4.8	6
26	Research advance in gas detection of volatile organic compounds released in rice quality deterioration process. Comprehensive Reviews in Food Science and Food Safety, 2021, 20, 5802-5828.	11.7	18
27	Friction of metal-matrix self-lubricating composites: Relationships among lubricant content, lubricating film coverage, and friction coefficient. Friction, 2020, 8, 517-530.	6.4	31
28	Deposition of hollow sphere In ₂ O ₃ coatings by liquid flame spray. Surface Engineering, 2020, 36, 1121-1127.	2.2	3
29	Microstructural features and compressive properties of SLM Ti6Al4V lattice structures. Surface and Coatings Technology, 2020, 403, 126419.	4.8	47
30	Synthesis and acetone sensing properties of copper (Cu2+) substituted zinc ferrite hollow micro-nanospheres. Ceramics International, 2020, 46, 28835-28843.	4.8	20
31	Effect of carbon content on microstructure, hardness and wear resistance of CoCrFeMnNiCx high-entropy alloys. Journal of Alloys and Compounds, 2020, 847, 156533.	5.5	86
32	ZnO1â^' coatings deposited by atmospheric plasma spraying for room temperature ppb-level NO2 detection. Applied Surface Science, 2020, 528, 147041.	6.1	13
33	Highly sensitive ZnO nanoparticles-loaded In2O3 hollow microsphere for detecting ppb-level NO2 at low working temperature. Progress in Natural Science: Materials International, 2020, 30, 469-476.	4.4	17
34	Microstructure and wear behavior of FeCoNiCrMn high entropy alloy coating deposited by plasma spraying. Surface and Coatings Technology, 2020, 385, 125430.	4.8	97
35	Micro-nano structured functional coatings deposited by liquid plasma spraying. Journal of Advanced Ceramics, 2020, 9, 517-534.	17.4	39
36	Recent Development of Corrosion Factors and Coating Applications in Biomass Firing Plants. Coatings, 2020, 10, 1001.	2.6	7

#	Article	IF	CITATIONS
37	Effect of Mo on tribological behaviors of atmospheric plasma sprayed Al2O3-13%TiO2/Mo coatings under boundary lubrication condition. Ceramics International, 2020, 46, 15066-15075.	4.8	19
38	Antibacterial properties of Magainin II peptide onto 304 stainless steel surfaces: A comparison study of two dopamine modification methods. Colloids and Surfaces B: Biointerfaces, 2020, 194, 111198.	5.0	20
39	Synthesis and NO2 sensing performances of CuO nanoparticles loaded In2O3 hollow spheres. Journal of Alloys and Compounds, 2020, 842, 155857.	5.5	33
40	Cavitation-corrosion behaviors of HVOF sprayed WC-25WB-10Co-5NiCr and MoB-25NiCr coatings. Ceramics International, 2020, 46, 21707-21718.	4.8	15
41	Ultrasensitive Gas Refractometer Using Capillary-Based Mach–Zehnder Interferometer. Sensors, 2020, 20, 1191.	3.8	9
42	Role of SiC nanoparticles on tribological properties of atmospheric plasma sprayed 5Âwt% SiC–Ni60 coatings. Tribology International, 2020, 146, 106220.	5.9	19
43	Microstructure and tribological properties of plasma sprayed FeCoNiCrSiAlx high entropy alloy coatings. Wear, 2020, 448-449, 203209.	3.1	53
44	Metal oxide semiconductors with highly concentrated oxygen vacancies for gas sensing materials: A review. Sensors and Actuators A: Physical, 2020, 309, 112026.	4.1	126
45	Facile synthesis and ppb-level H2S sensing performance of hierarchical CuO microflowers assembled with nano-spindles. Journal of Materials Science: Materials in Electronics, 2020, 31, 7937-7945.	2.2	16
46	Wear mechanism of Cu-based brake pad for high-speed train braking at speed of 380Âkm/h. Tribology International, 2020, 150, 106357.	5.9	60
47	SLURRY EROSION BEHAVIOR OF HVOF SPRAYED WC-12Co AND Cr3C2-25NiCr COATINGS DEPOSITED ON 16Cr5Ni STAINLESS STEEL. Surface Review and Letters, 2020, 27, 1950193.	1.1	2
48	Modification of a derived antimicrobial peptide on steel surface for marine bacterial resistance. Applied Surface Science, 2020, 510, 145512.	6.1	31
49	Structure and Photocatalytic Properties of TiO2 Coated Multi-Walled Carbon Nanotubes Prepared by Solvothermal Method. ECS Journal of Solid State Science and Technology, 2020, 9, 063001.	1.8	2
50	Effect of Heat Treatment on the Cavitation Erosion Performance of WC–12Co Coatings. Coatings, 2019, 9, 690.	2.6	13
51	Wear and corrosion resistant performance of thermal-sprayed Fe-based amorphous coatings: A review. Surface and Coatings Technology, 2019, 377, 124896.	4.8	133
52	A spherical surface coating thickness model for a robotized thermal spray system. Robotics and Computer-Integrated Manufacturing, 2019, 59, 297-304.	9.9	17
53	Zinc ferrite based gas sensors: A review. Ceramics International, 2019, 45, 11143-11157.	4.8	116
54	Room temperature conductive type metal oxide semiconductor gas sensors for NO2 detection. Sensors and Actuators A: Physical, 2019, 289, 118-133.	4.1	143

#	Article	IF	CITATIONS
55	Synthesis and acetone sensing properties of ZnFe ₂ O ₄ /rGO gas sensors. Beilstein Journal of Nanotechnology, 2019, 10, 2516-2526.	2.8	24
56	Microstructure, wear and corrosion behaviors of plasma sprayed NiCrBSi-Zr coating. Surface and Coatings Technology, 2019, 360, 172-180.	4.8	36
57	Visible light enhanced black NiO sensors for ppb-level NO2 detection at room temperature. Ceramics International, 2019, 45, 4253-4261.	4.8	63
58	Room-temperature NO2 gas sensors based on rGO@ZnO1-x composites: Experiments and molecular dynamics simulation. Sensors and Actuators B: Chemical, 2019, 282, 690-702.	7.8	97
59	Pt-activated TiO2-MoS2 nanocomposites for H2 detection at low temperature. Journal of Alloys and Compounds, 2018, 747, 550-557.	5.5	41
60	Modeling of Thickness and Profile Uniformity of Thermally Sprayed Coatings Deposited on Cylinders. Journal of Thermal Spray Technology, 2018, 27, 288-295.	3.1	7
61	Solution precursor plasma sprayed tungsten oxide particles and coatings. Materials and Manufacturing Processes, 2018, 33, 1107-1114.	4.7	7
62	Microstructure and tribological properties of plasma sprayed Cu-15Ni-8Sn coatings. Surface and Coatings Technology, 2018, 337, 159-167.	4.8	32
63	Effects of temperature and atmosphere on microstructure and tribological properties of plasma sprayed FeCrBSi coatings. Journal of Alloys and Compounds, 2018, 753, 586-594.	5.5	20
64	Graphene-enhanced metal oxide gas sensors at room temperature: a review. Beilstein Journal of Nanotechnology, 2018, 9, 2832-2844.	2.8	126
65	Switching Brake Materials To Extremely Wear-Resistant Self-Lubrication Materials via Tuning Interface Nanostructures. ACS Applied Materials & Interfaces, 2018, 10, 19173-19181.	8.0	28
66	Microstructure evolution and tribological performance of Cu-WS2 self-lubricating composites. Wear, 2018, 412-413, 109-119.	3.1	49
67	In-situ TiC-Graphite-Ni hybrid composites innovatively fabricated by pressureless reactive infiltration method. Journal of Alloys and Compounds, 2018, 757, 273-278.	5.5	2
68	Synthesis and acetone gas sensing properties of Ag activated hollow sphere structured ZnFe2O4. Ceramics International, 2018, 44, 20700-20707.	4.8	53
69	Molecularly imprinted electropolymerization on a metal-coated optical fiber for gas sensing applications. Sensors and Actuators B: Chemical, 2017, 244, 1145-1151.	7.8	61
70	Preparation and characterization of CuxO1-y@ZnO1-α nanocomposites for enhanced room-temperature NO2 sensing applications. Applied Surface Science, 2017, 401, 248-255.	6.1	26
71	Visible light assisted nitrogen dioxide sensing using tungsten oxideÂ-ÂGraphene oxide nanocomposite sensors. Materials Chemistry and Physics, 2017, 191, 114-120.	4.0	28
72	Light assisted room-temperature NO 2 sensors with enhanced performance based on black SnO 1-α @ZnO 1-β @SnO 2-γ nanocomposite coatings deposited by solution precursor plasma spray. Ceramics International, 2017, 43, 5990-5998.	4.8	18

#	Article	IF	CITATIONS
73	Suspension Plasma-Sprayed ZnFe2O4 Nanostructured Coatings for ppm-Level Acetone Detection. Journal of Thermal Spray Technology, 2017, 26, 728-734.	3.1	18
74	Role of oxygen vacancy in tuning of optical, electrical and NO2 sensing properties of ZnO1-x coatings at room temperature. Sensors and Actuators B: Chemical, 2017, 248, 886-893.	7.8	102
75	Tribological behavior of copper-molybdenum disulfide composites. Wear, 2017, 384-385, 61-71.	3.1	54
76	Flexible NO 2 gas sensors based on sheet-like hierarchical ZnO 1â^' x coatings deposited on polypropylene papers by suspension flame spraying. Journal of the Taiwan Institute of Chemical Engineers, 2017, 75, 280-286.	5.3	22
77	Photon assisted room-temperature hydrogen sensors using PdO loaded WO 3 nanohybrids. International Journal of Hydrogen Energy, 2017, 42, 6425-6434.	7.1	46
78	Role of Mo on tribological properties of atmospheric plasma-sprayed Mo-NiCrBSi composite coatings under dry and oil-lubricated conditions. Journal of Alloys and Compounds, 2017, 727, 841-850.	5.5	47
79	Effect of heat treatment on structure and property evolutions of atmospheric plasma sprayed NiCrBSi coatings. Surface and Coatings Technology, 2017, 325, 548-554.	4.8	80
80	Comparative study on tribological mechanisms of polyimide composites when sliding against medium carbon steel and NiCrBSi. Journal of Colloid and Interface Science, 2017, 506, 415-428.	9.4	36
81	Investigation of the crystallinity of suspension plasma sprayed hydroxyapatite coatings. Journal of the European Ceramic Society, 2017, 37, 5017-5021.	5.7	51
82	Hydrogen sensors based on noble metal doped metal-oxide semiconductor: A review. International Journal of Hydrogen Energy, 2017, 42, 20386-20397.	7.1	213
83	Effects of laser shock processing on corrosion resistance of AISI 304 stainless steel in acid chloride solution. Journal of Alloys and Compounds, 2017, 723, 237-242.	5.5	34
84	Room-temperature nitrogen-dioxide sensors based on ZnO1â^'x coatings deposited by solution precursor plasma spray. Sensors and Actuators B: Chemical, 2017, 242, 102-111.	7.8	65
85	Microstructure and sensing properties of CdS-ZnO1â^'x coatings deposited by liquid plasma spray and treated with hydrogen peroxide solution for nitrogen dioxide detection at room temperature. Journal of Alloys and Compounds, 2016, 687, 286-293.	5.5	42
86	Sliding electrical contact behavior of brass fiber brush against coin-silver and Au plating. Wear, 2016, 368-369, 461-469.	3.1	24
87	Acetaldehyde Chemical Sensor based on Molecularly Imprinted Polypyrrole. Procedia Engineering, 2016, 168, 569-573.	1.2	8
88	Deposition of Nanostructured Fluorineâ€Doped Hydroxyapatite Coating from Aqueous Dispersion by Suspension Plasma Spray. Journal of the American Ceramic Society, 2016, 99, 2899-2904.	3.8	9
89	Effect of Spray Distance on Microstructure and Tribological Performance of Suspension Plasma-Sprayed Hydroxyapatite–Titania Composite Coatings. Journal of Thermal Spray Technology, 2016, 25, 1255-1263.	3.1	21
90	Cadmium sulfide activated zinc oxide coatings deposited by liquid plasma spray for room temperature nitrogen dioxide detection under visible light illumination. Ceramics International, 2016, 42, 4845-4852.	4.8	57

#	Article	IF	CITATIONS
91	Tungsten oxide coatings deposited by plasma spray using powder and solution precursor for detection of nitrogen dioxide gas. Journal of Alloys and Compounds, 2016, 668, 128-136.	5.5	22
92	Deposition, nanostructure and phase composition of suspension plasma-sprayed hydroxyapatite coatings. Ceramics International, 2016, 42, 8684-8690.	4.8	29
93	Room temperature nitrogen dioxide sensors based on N719-dye sensitized amorphous zinc oxide sensors performed under visible-light illumination. Sensors and Actuators B: Chemical, 2015, 209, 69-77.	7.8	56
94	Microstructure and gas sensing properties of solution precursor plasma-sprayed zinc oxide coatings. Materials Research Bulletin, 2015, 63, 67-71.	5.2	30
95	Palladium nanoparticle deposition via precipitation: a new method to functionalize macroporous silicon. Science and Technology of Advanced Materials, 2014, 15, 065002.	6.1	4
96	Solution precursor plasma-sprayed tungsten oxide coatings for nitrogen dioxide detection. Ceramics International, 2014, 40, 11427-11431.	4.8	25
97	Sensing mechanism of hydrogen sensors based on palladium-loaded tungsten oxide (Pd–WO3). Sensors and Actuators B: Chemical, 2013, 187, 84-93.	7.8	78
98	Room temperature responses of visible-light illuminated WO3 sensors to NO2 in sub-ppm range. Sensors and Actuators B: Chemical, 2013, 181, 395-401.	7.8	129
99	Sensitive and rapid hydrogen sensors based on Pd–WO3 thick films with different morphologies. International Journal of Hydrogen Energy, 2013, 38, 2565-2577.	7.1	82
100	H2 sensors based on WO3 thin films activated by platinum nanoparticles synthesized by electroless process. International Journal of Hydrogen Energy, 2013, 38, 2929-2935.	7.1	52
101	N719-dye sensitized amorphous zinc oxide films for NO <inf>2</inf> detection under visible-light illumination. , 2013, , .		1
102	High-refractive-index transparent coatings enhance the optical fiber cladding modes refractometric sensitivity. Optics Express, 2013, 21, 29073.	3.4	45
103	Polarization dependency in metal oxide coated tilted FBG refractometers. Proceedings of SPIE, 2012, , .	0.8	Ο
104	Thickness influence on the polarization dependency of tilted fiber Bragg gratings coated by zinc oxide thin films. , 2012, , .		0
105	SO2 Gas Sensors based on WO3 Nanostructures with Different Morphologies. Procedia Engineering, 2012, 47, 1033-1036.	1.2	37
106	Visible Light Activated Tungsten Oxide Sensors for NO2 Detection at Room Temperature. Procedia Engineering, 2012, 47, 116-119.	1.2	11
107	Sensing properties of Pt/Pd activated tungsten oxide films grown by simultaneous radio-frequency sputtering to reducing gases. Sensors and Actuators B: Chemical, 2012, 175, 53-59.	7.8	30
108	Hydrothermal Synthesis of Two Dimensional WO3 Nanostructures for NO2 Detection in the ppb-level. Procedia Engineering, 2012, 47, 228-231.	1.2	17

#	Article	IF	CITATIONS
109	Improvement of sensing characteristics of radio-frequency sputtered tungsten oxide films through surface modification by laser irradiation. Materials Chemistry and Physics, 2012, 133, 588-591.	4.0	17
110	Study of selectivity of NO2 sensors composed of WO3 and MnO2 thin films grown by radio frequency sputtering. Sensors and Actuators B: Chemical, 2012, 161, 914-922.	7.8	30
111	Magnetron sputtered tungsten oxide films activated by dip-coated platinum for ppm-level hydrogen detection. Thin Solid Films, 2012, 520, 3679-3683.	1.8	20
112	Hydrogen sensors based on Pd-doped WO3 nanostructures and the morphology investigation for their sensing performances optimization. Procedia Engineering, 2011, 25, 264-267.	1.2	8
113	Using co-sputtered platinum or palladium activated tungsten oxide films to detect reducing gases. Procedia Engineering, 2011, 25, 823-826.	1.2	1
114	Improvement in selectivity of NO <inf>2</inf> sensors based on WO <inf>3</inf> thin films with MnO <inf>2</inf> filters deposited by radio frequency sputtering. , 2011, , .		0
115	Effect of vacuum heat treatment on tensile strength and fracture performance of cold-sprayed Cu-4Cr-2Nb coatings. Applied Surface Science, 2011, 257, 5972-5976.	6.1	14
116	Highly sensitive hydrogen sensors based on co-sputtered platinum-activated tungsten oxide films. International Journal of Hydrogen Energy, 2011, 36, 1107-1114.	7.1	71
117	Sensing properties of atmospheric plasma-sprayed WO3 coating for sub-ppm NO2 detection. Sensors and Actuators B: Chemical, 2010, 144, 280-288.	7.8	140
118	Preparation of highly selective, sensitive and stable hydrogen sensors based on Pd-doped tungsten trioxide. Procedia Engineering, 2010, 5, 180-183.	1.2	29
119	Deposition and microstructure characterization of atmospheric plasma-sprayed ZnO coatings for NO2 detection. Applied Surface Science, 2010, 256, 5905-5910.	6.1	54
120	Microstructure and mechanical properties of flame-sprayed PEEK coating remelted by laser process. Progress in Organic Coatings, 2009, 66, 248-253.	3.9	37
121	Effect of in-flight particle characteristics on the coating properties of atmospheric plasma-sprayed 8mol% Y2O3–ZrO2 electrolyte coating studying by artificial neural networks. Surface and Coatings Technology, 2009, 204, 463-469.	4.8	25
122	Effect of heat treatment on microstructure and mechanical properties of cold sprayed Ti coatings with relatively large powder particles. Journal of Coatings Technology Research, 2009, 6, 401-406.	2.5	31
123	Modeling Aspects of High Velocity Impact of Particles in Cold Spraying by Explicit Finite Element Analysis. Journal of Thermal Spray Technology, 2009, 18, 921-933.	3.1	92
124	Study on gas permeation behaviour through atmospheric plasma-sprayed yttria stabilized zirconia coating. Surface and Coatings Technology, 2008, 202, 5055-5061.	4.8	41
125	Effect of Ball Milling of Feedstock Powder on Microstructure and Properties of TiN Particle-Reinforced Al Alloy-Based Composites Fabricated by Cold Spraying. Journal of Thermal Spray Technology, 2008, 17, 316-322.	3.1	42
126	Effect of standoff distance on coating deposition characteristics in cold spraying. Materials & Design, 2008, 29, 297-304.	5.1	99

#	Article	IF	CITATIONS
127	Microwave sintering of plasma-sprayed yttria stabilized zirconia electrolyte coating. Journal of the European Ceramic Society, 2008, 28, 2529-2538.	5.7	13
128	Temperature dependence of the tribological mechanisms of amorphous PEEK (polyetheretherketone) under dry sliding conditions. Acta Materialia, 2008, 56, 2182-2190.	7.9	72
129	Effect of in-flight particle velocity on the performance of plasma-sprayed YSZ electrolyte coating for solid oxide fuel cells. Surface and Coatings Technology, 2008, 202, 2654-2660.	4.8	32
130	Characterizations of cold-sprayed Nickel–Alumina composite coating with relatively large Nickel-coated Alumina powder. Surface and Coatings Technology, 2008, 202, 4855-4860.	4.8	61
131	Effects of sliding velocity and applied load on the tribological mechanism of amorphous poly-ether–ether–ketone (PEEK). Tribology International, 2008, 41, 79-86.	5.9	72
132	Synthesis of Lanthanum Silicates Electrolyte for Intermediate Temperature SOFC. ECS Transactions, 2007, 7, 2351-2355.	0.5	0
133	Ti and Ti-6Al-4V Coatings by Cold Spraying and Microstructure Modification by Heat Treatment. Advanced Engineering Materials, 2007, 9, 418-423.	3.5	86
134	Study on impact fusion at particle interfaces and its effect on coating microstructure in cold spraying. Applied Surface Science, 2007, 254, 517-526.	6.1	103
135	Ionic conductivity and its temperature dependence of atmospheric plasma-sprayed yttria stabilized zirconia electrolyte. Materials Science and Engineering B: Solid-State Materials for Advanced Technology, 2007, 137, 24-30.	3.5	112
136	Structures and tribological performances of PEEK (poly-ether-ether-ketone)-based coatings designed for tribological application. Progress in Organic Coatings, 2007, 60, 39-44.	3.9	63
137	Microstructure and Electrical Conductivity of Atmospheric Plasma-Sprayed LSM/YSZ Composite Cathode Materials. Journal of Thermal Spray Technology, 2007, 16, 1005-1010.	3.1	11
138	Significant influences of metal reactivity and oxide films at particle surfaces on coating microstructure in cold spraying. Applied Surface Science, 2007, 253, 3557-3562.	6.1	82
139	Deposition characteristics of Al–12Si alloy coating fabricated by cold spraying with relatively large powder particles. Applied Surface Science, 2007, 253, 7124-7130.	6.1	30
140	Characterization of atmospheric plasma-sprayed Sc2O3–ZrO2 electrolyte coating. Solid State Ionics, 2006, 177, 2149-2153.	2.7	17
141	Characterization of YSZ Solid Oxide Fuel Cells Electrolyte Deposited by Atmospheric Plasma Spraying and Low Pressure Plasma Spraying. Journal of Thermal Spray Technology, 2006, 15, 598-603.	3.1	37
142	Microstructure and Wear Behavior of SiC _P -Reinforced Magnesium Matrix Composite by Cold Spraying. Advanced Materials Research, 0, 314-316, 253-258.	0.3	0